We are IntechOpen,
the world's leading publisher of Open Access books
Built by scientists, for scientists

6,000
Open access books available

148,000
International authors and editors

185M
Downloads

154
Countries delivered to

Our authors are among the

TOP 1%
most cited scientists

12.2%
Contributors from top 500 universities

CLARIVATE ANALYTICS
BOOK CITATION INDEX
INDEXED

WEB OF SCIENCE™

Selection of our books indexed in the Book Citation Index
in Web of Science™ Core Collection (BKCI)

Interested in publishing with us?
Contact book.department@intechopen.com

Numbers displayed above are based on latest data collected.
For more information visit www.intechopen.com

Chapter

Recent Advances in Oil-Spill Monitoring Using Drone-Based Radar Remote Sensing

Bilal Hammoud and Norbert Wehn

Abstract

Oil spills are regrettably common and have socioeconomic implications on communities and disastrous consequences on the marine ecosystem and maritime life. The European Space Agency (ESA) has stated that worldwide spillage exceeds 4.5 million tons of oil annually, where 45% of the amount is due to operative discharges from ships. To alleviate the severity of oil spills and promptly react to such incidents, it is crucial to have oil-spill monitoring systems, which enable an effective contingency plan to dictate the best actions for dealing with oil spills. A quick and efficient intervention requires the (1) detection of oil slicks, (2) thickness estimation, and (3) oil classification. The European Maritime Safety Agency (EMSA) highlighted in 2016 the need to use drones as complementary systems supporting satellite maritime surveillance. While multiple sensors could be used, active radars appear to be prominent for oil spill monitoring. In this chapter, we present recent advances in drone-based radar remote sensing as an effective oil spill monitoring system. It shows from the system-level perspective the capability of radar systems on drones, using high spectral resolution and parallel scanning, to perform the above-required functionalities (1, 2, and 3) and provide valuable information to contain the damage.

Keywords: oil spills, drone, radar, reflectivity, slick detection, thickness estimation, classification

1. Introduction to oil spills: Sources, effects, and reaction

Petroleum products are used across the globe by most industries and for different applications, where the requirement for the presence of petroleum materials on site is often imperative. This need stresses the necessity of moving petroleum substances using maritime ships or underwater pipelines internationally between different continents and countries. To move the oil from its source to the final consumer, up to 15 transfers are involved [1, 2]. Several reasons could cause the occurrence of oil spills: in addition to the intentional petroleum waste spill in seawater, transportation is vulnerable to involuntary oil spills from tanker collisions with rocky shoals, ship accidents, and pipeline ruptures [3]. On a global scale, the European Space Agency (ESA) has stated that the worldwide spillage exceeds 4.5 million tons of oil annually, where

45% of the amount is due to operative discharges from ships [4]. Accordingly, spills in seawater including light oil, gasoline, fuel, crude oil, and bulk oil have adverse long-term repercussions on the maritime environment. They happen on a global scale, influence maritime and human life, and have socioeconomic implications on communities [5, 6]. Depending on the ocean state and seawater currents, an oil spill can scatter over a very wide area in the open sea within only a few hours. Once the spill occurs, the oil quickly spreads to form a thick slick that becomes thinner over time when moving away from the source. This thin layer is called a "sheen" and has a rainbow-like appearance [1]. Therefore, oil spills can have varying thicknesses, ranging from less than a micrometer (um) for sheens to millimeters (mm) for thick slicks as documented in the Deep-Water Horizon case field samples [7, 8]. Based on the oil type and its thickness, a slick can evaporate quickly or can persist in the environment for a long time. For example, even though light oils are highly toxic, they evaporate quickly. But heavy oils, which are less toxic, persist in seawater for a much longer time and can get mixed with pebbles and sandy beaches where they remain for years [1]. Worldwide, fuels and crude oils account for 48% and 29% of the total oil spilled into the seawater, respectively, highlighting again how much the impact on the environment could be severe [9].

In the last decades, thousands of tons of oil were spilled worldwide. The quantity of oil spilled from tankers in the 1990s is estimated to be more than 1.13 million tons of oil, while 73% of the total amount occurred in 10 incidents only [10]. For example, during the Gulf War spill that occurred in 1991 on the sea island in Kuwait, around 800,000 tons of heavy crude oil were released from storage and ships [11]. Another huge spill occurred in 1992 in Fergana Valley in Uzbekistan due to an oil well blowout. During this accident, the estimation of the spilled oil is around 300,000 tons [2]. According to the international tanker owners' pollution federation (ITOPF), the estimated amount of oil spilled from tankers in the 2000s is 196,000 tons [10]. In 2010, while 4000 tons of diluted bitumen were spilled in Kalamazoo, Michigan, due to a pipeline rupture, an approximation of 500,000 tons of light crude oil were spilled in the same year in the Gulf of Mexico due to an oil well blowout [11]. Very recently in 2018, an oil spill of 113,000 tons size happened off Shanghai in China [10] in the Sanchi oil tanker collision.

While environmental rules, regulations, and strict operating procedures have been imposed to prevent oil spills, these measures cannot completely eliminate the risk [2]. Therefore, there is a need to set up oil spill contingency plans in countries where the chances of such disasters are high. These plans are usually prepared by the petroleum administration in close cooperation with ministries, governmental and non-governmental organizations as well as regional and international entities. They aim to protect human life, natural resources, and the economy by preserving the coastal and marine environment from any adverse effects an oil spill might pose. The main objective of such plans is to maintain the alertness and readiness of the involved entities to ensure a timely and effective response to oil spills and to prevent further pollution. In most scenarios, it requires the quick mobilization of aerial surveillance resources and consultation with international remote sensing institutions to provide oil spill modeling data or remote sensing images. Accordingly, to permit a swift and appropriate reaction and limit contamination, a need to establish an effective oil spill monitoring system presents itself in utmost urgency.

The contingency plan deals with various transformation processes including weathering, evaporation, and emulsification that occur when the oil is spilled on water. Also, the plan considers oil movements in seawater given the oil's physical

characteristics and how it interacts with ocean waves. To contain the oil and prevent its spread over time, special equipment such as booms is used on-site. Afterward, devices such as skimmers and absorbing material such as sorbents are used to recover oil from the surface. Other alternatives are to use surface-washing and chemical dispersant agents to treat the oil or to have in-situ controlled burning as a cleanup technique [2]. All previous measures are very critical to making the contingency plan very effective. But a necessary factor for their usefulness is the pre-knowledge that is available about the spill. The more information is collected from the spill scene, the better the measures used for containment and cleaning-up operations are. The first and most critical information is the spill location. Other information, including the volume spilled or the type of the oil, is also necessary to define proper measures in the contingency plan. Since this information is not available at an early stage in many spills, surface techniques, as well as remote sensing techniques, are frequently used for the first assessment and evaluation.

Remote sensing is the field that combines science and technology to extract ("sense") information about an object or phenomenon at a distance ("remotely") by instrument-based techniques. A detailed description of the state-of-the-art remote sensing technologies for oil spill surveillance is listed in [1, 12–14]. The sensors used are usually mounted on aircraft or satellite platforms. They target the detection, thickness estimation, classification, or a combination of these functionalities. As an addition to the state-of-the-art systems, the aim of this chapter is to present a new advancement in oil spill monitoring using drone-based radar remote sensing, which complements currently available systems for better oil spill surveillance. Section 2 provides an overview of the oil spill monitoring system and gives the necessary background about the techniques used up to now for monitoring. It describes the pros and cons of the sensors (2.1) and platforms (2.2) used by state-of-the-art techniques to monitor oil spills. Furthermore, it describes the required information (2.3) and the main features (2.4) for good monitoring and an effective contingency plan. In addition, a system-level view of the new drone-based proposed solution is presented (2.5) and compared with recently developed state-of-the-art techniques in terms of their functionalities and the used sensors (2.6). Section 3 elaborates more on the new proposed approach for oil spill monitoring for oil spill detection, estimation, and classification. It describes in detail the system model (3.1), the new probabilistic detection algorithms (3.2), the new statistical thickness estimation algorithms (3.3), and the neural network regression algorithm for the oil type classification (3.4). The feature of onboard processing is elaborated more (3.5), and the system-level complementary solution is described (3.6). Section 4 concludes this chapter by summarizing the importance of the presented approach as a complementary solution to state-of--the-art techniques and highlights new aspects that should be considered in future developments.

2. Oil spill monitoring system

In this section, we present a brief overview of the state-of-the-art techniques used for oil spill monitoring in relation to the sensors used and to the platforms operated during the oil spill. Then, we motivate our new proposed solution by listing the system features, the required functionalities for an effective contingency plan, and how our solution differs from relevant state-of-the-art techniques. For more details about oil spill surveillance systems, the reader is encouraged to refer to [12–14].

2.1 Sensors

2.1.1 Visual sensors

Despite many shortcomings, passive sensors that operate in the visible region of the light are still used in oil spill remote sensing. The effect of some environmental conditions such as sun glint and wind sheen would lead to a misinterpretation by creating a resemblance to oil sheens, which is considered a limitation of such sensors [1]. Another drawback is that visual sensors cannot operate at night because they are using sunlight reflectance for operation. In addition, they require cloudless and clear weather requirements. Given the limitations of visual sensors for oil spill detection, and since they are not able to provide thickness information or oil classification, these sensors are not used alone for oil spill monitoring. For example, in [15], optical remote sensing images are combined with visible infrared imager radiometer suite (VIIRS) images in a semi-automatic fashion to extract oil slick features. The technique is tested in the North-West of the Gulf of Mexico. However, this method cannot be fully automated and requires human intervention to set a proper threshold for feature extraction. Optical sensors are rather used to document the spill and to provide a frame of reference for other sensors [16, 17].

2.1.2 Infrared sensors

Infrared passive sensors are relatively cheap remote-sensing technologies that can be used to detect oil spills [18]. The emissivity of the oil in the thermal infrared red region is lower than the emissivity of the water. This is how the thick oil could be distinguished from the background water by absorbing the infrared radiation from the sun and appearing as a hot spot compared with the cold background for the water [1]. An opposite phenomenon is observed during the night when the heat loss from the oil layer is faster compared with the water. This is the reason why they appear cooler at night [19]. However, false-positive results could be obtained by misinterpreting the thermal radiation from seaweeds. In addition, infrared sensors require the absence of cloud and heavy fog for good operation [1, 2, 20]. Infrared sensors can detect oil films with 10s–100 s um thickness. However, the brightness of the infrared sensing-based imagery does not vary with slick thicknesses in the mm range. Therefore, we cannot rely on infrared sensors to yield slick thickness measurements [13, 21, 22]. [23] shows that thermal infrared sensors that are mounted on helicopters can detect oil spills in the accident of the Dalian Xingang oil pipeline explosion in July 2010. Similarly, [24] shows that using MODIS thermal infrared data, the information obtained from the sea surface temperature identifies the oil film from seawater. This technique is applied to the Jiyyeh spill when Israel bombarded storage tanks in Lebanon during the war of 2006, where around 15,000 tons of heavy fuel oil spilled into the Mediterranean Sea [24, 25].

2.1.3 Ultraviolet sensors

Very thin oil films have a strong reflectance in the ultraviolet region compared with seawater. This allows the use of ultraviolet sensors for oil spill detection when the thickness is not greater than 10 um. Also, look-alikes such as sun glints, wind slicks, and biogenic material challenge ultraviolet sensors for oil spill detection [1, 3]. [26] proposed adaptive thresholding for chemical spill detection (not oil specifically) from

ultraviolet images, which shows a distinction between the chemicals and the water background. [27] used ultraviolet range for remote detection of hydrocarbons such as benzene. Generally, fewer ultraviolet sensors are being used for oil spills in today's remote sensing because of the low relevance of thin slicks to oil spill cleanup [3, 13, 28].

2.1.4 Passive microwave radiometer sensors

Compared with water, the oil emits stronger microwave radiation and appears brighter in the background. Passive microwave radiometers [29–32] are used for both oil spill detection and thickness estimation [13]. The need to acquire knowledge about weather conditions, the low spatial resolution of this sensor, and the a-priori knowledge required about the oil characteristics all influence the microwave brightness and decrease the effectiveness of microwave radiometers for oil spill monitoring [1]. Furthermore, the main issue with this technology tends to be the cyclical relationship between the microwave brightness of the slick and its thickness. Currently, available models can only measure limited thickness ranges [14]. For example, using a multi-frequency passive microwave radiometer, the measured thickness range is limited between 0.1 and 1.5 mm as reported in [33], or the results were underestimating the real thickness values as in [30] where the calibration methodology and the selection of frequencies limited the measured thickness to a maximum of 1 mm. The only commercial tools currently available for measuring slick thickness are the Optimare 3–5-channel microwave instruments. They can provide thickness up to 3 mm only [13]. Given the requirement of a dedicated aircraft to mount this sensor, in addition to their high cost, it is complicated to put them into operation. Currently, the microwave sensor is not being used for oil detection and slick imaging [13].

2.1.5 Radar sensors

With the absence of oil slicks, a bright image is obtained by radar sensors for clean seawater. Once the oil is spilled into seawater, the ocean capillary waves are reduced, and radar reflections are decreasing. Dark spots are obtained in radar imaging. This allows for oil spill detection [34]. Synthetic aperture radar (SAR) and side-looking airborne radar (SLAR) are the two most common types of radar, which are used for oil spill remote sensing [35]. Imaging SAR systems [36–39] are off-nadir instruments whose backscattering over the ocean is primarily due to Bragg scattering at relevant incident angles. The synthetic aperture radar technique is highly prone to false targets, however, and is limited to a narrow range of wind speeds when small ocean waves do not yield a difference between the oiled area and the sea [2]. SAR techniques are not used for oil thickness estimations nor for oil classification. Being widely mounted on space-borne platforms, the radar is a very useful active sensor for a synoptic view of the oil spill over a wide scene [1].

2.2 Platforms: Airborne to satellites to complementary drones

Most recent techniques using one sensor, or a combination of sensors, are done remotely using airborne systems [40, 41] or satellites [42–47]. Radar satellites provide a selection of resolutions and polarizations [13]. Serious efforts have been made to replace airborne remote sensing with satellite remote sensing. However, satellites face the limitations of overpass frequency and low spatial resolution [12], and the long

time required for processing the dataset, potentially disrupting oil spill contingency planning. This limitation has been improved using satellite constellations. A revisit time within a few hours can be provided by a larger number of SAR satellites. Airborne systems, despite their high cost due to aircraft dedication, can be used directly when needed for real-time dataset processing [1]. In addition, they provide flexibility in terms of deployment time and choices of sensors. Therefore, a combination of satellite and airborne sensors is used in many countries in northern Europe for oil spill surveillance. The strategic planning is based on satellite imagery that provides a synoptic view of the oil spill, whereas airborne sensors are used for short-term or tactical responses [9]. Contrarily to visible and radar sensors, due to the high atmospheric absorption and scattering, many sensors including the infrared and the fluorosensors are not suitable to be operated on a space-borne platform [34, 48].

Despite all the effort done using space-borne platforms, only 25% of the pollution cases are detected by satellite systems. For a quick response and rapid intervention, the European Maritime Safety Agency (EMSA) has proposed using drones as complementary systems in satellite maritime surveillance [49]. Aerial surveillance could be improved significantly through the introduction of drones because it is a quick assessment tool for oil spill accidents [50]. In addition, drone-based tools will be particularly valuable as it provides high spectral resolution, at a relatively low cost.

2.3 Required information

Once a spill occurs, the oil will spread quickly on the water surface to form oil layers such as slicks, films, and sheens. To alleviate the severity of oil spills and promptly react to such incidents, it is crucial to have oil-spill monitoring systems that enable an effective contingency plan [51]. A rapid response time and a quick intervention allow dictating the best actions to deal with oil spills. Therefore, monitoring systems must perform several functionalities and provide valuable information to contain the damage [52].

1. Functionality #1: Oil-spill detection

   The most important part during oil spills is to detect oil slicks. It is important to locate them and to determine how large the spread is. This necessary information allows oil spill mapping for both tactical and strategic countermeasures.

2. Functionality #2: Oil-thickness estimation

   The thickness distribution of spilled oil is another critical information for spill containment. Using the knowledge about the oil thickness, an estimation of the total volume spilled can be performed so that adequate tools are used in cleanup operations.

3. Functionality #3: Oil classification

   Classifying the oil type is also important during spill containment. Based on this information, the authorities estimate the environmental damage in the short- and long term to take appropriate response activities.

4. Functionality #4: Oil-spill tracking

Since the spill can spread quickly within a few hours, an effective contingency plan demands the ability to track the spill over time. Tracking provides timely and valuable information to anticipate possible damage scenarios, predict the trajectory using additional input from weather forecasts, and assist in cleanup operations.

2.4 Features for good monitoring

In addition to the four functionalities included in the previous section, it is also important to take the following system requirements [1] into consideration whenever an effective oil spill monitoring system is designed. This allows for selecting properly the sensor and the platform. In addition, suitable and effective algorithms could be developed.

- *Spatial resolution*: it is an important characteristic of the sensor that affects the accuracy in mapping oil slicks with accurate thickness measurements.

- *Quick response*: oil spill surveillance requires an acceptable time frame for collecting and processing the data, which stresses the need for real-time data availability.

- *Day-time conditions*: the operation of the sensor at any time during the day and night is essential for an effective surveillance system.

- *weather conditions*: it is important to limit the effects of weather conditions including rain and fog.

- *Large-scale view*: the sensor that captures a synoptic view of the area allows monitoring over a large spill spread.

- *Cost and size*: the acceptable size and cost of the sensor are critical to decreasing the overall cost of the system.

2.5 New proposed solution: Wide-band radar on drone platforms

Based on the previous criteria, visible and ultraviolet cannot work at night. Moreover, infrared sensors cannot provide estimations of thicknesses. Therefore, we select radar sensors for the proposed monitoring system because they operate during the day and night and under all weather conditions. Whenever mounted on satellites, radar is a very useful active sensor to detect oil over a large area. However, the synthetic aperture radar technique is limited to a narrow range of wind speeds. The ocean's slight surface roughness due to very low wind speeds (below 4 m/s) leads the backscattering to be dominated by the specular component, challenging SAR systems for oil spill detection [38]. Therefore, it would be advantageous to study the radar observations from nadir-looking systems (transmit and receive at zero angles from the normal to the ocean surface) since they cover scenarios that cannot be studied by SAR systems. Being largely independent of surface roughness, the returns from nadir (or near-nadir) systems will benefit from the dominance of the specular scattering and enable detection in very low wind conditions. Therefore, drone platforms are designated suitable for the proposed solution. The drone-based radar solution allows quick

assessment of the area where the flag of possible spills is raised by witnesses. As a drawback, operating these platforms as nadir-looking systems decreases the surface of the scanned area viewed by the radar compared with that scanned by "side-looking" platforms. Also, using drones instead of satellites does not allow a synoptic view of the spill. But this can be compensated by using multiple drones at a time instead of scanning with a single drone. The parallelization in scanning can cover a large area at a critical time. Once a possible oil spill is announced, the drones can be directly used as tactical-response systems to scan the scene and report results. Afterward, whenever the spill is confirmed, the satellites can be used for strategic planning by providing a synoptic view of the spill area. Furthermore, scanning with drones provides a high spatial resolution compared with satellites and with a principal advantage of a relatively low cost compared with dedicated airborne detection systems.

Hence, we propose a new approach for oil spill monitoring with the following features, which are discussed in more detail in Section 3:

1. From a system-level perspective, we suggest the incorporation of both C-band and X-band using remote sensing nadir-looking wide-band radar sensors that can be implemented on drones as oil spill monitoring systems.

2. Our new approach targets the spills happening during calm and moderate ocean conditions, which are challenging for state-of-the-art SAR systems.

3. Compared with the state-of-the-art techniques, the newly proposed system implements maximum-Likelihood and machine learning statistical algorithms that can perform simultaneously in real time:

   a. functionality #1 by detecting thick oil slicks

   b. functionality #2 by estimating the thicknesses of detected slicks in the mm range

   c. functionality #3 by classifying the oil type

The proposed solution is not intended to replace state-of-the-art techniques but rather complements them by providing a complementary system to satellite SAR systems. During the early stages of a possible oil spill, drone systems act as small-scale tactical-response systems improving the large-scale surveillance obtained by satellite systems. Over the spill duration and based on satellite scans, the drones can track the spill using the high spatial resolution feature provided by the mounted wide-band radars.

2.6 Comparison to latest state-of-the-art techniques[1]

Several state-of-the-art techniques have been already included when we introduced the sensors (Section 2.1) and platforms (Section 2.2). To follow up on Section 2.5 where we describe the importance of the proposed approach—and for convenience

---

[1] It is important to keep in mind that in this section we are not including all state-of-the-art techniques used for oil spill monitoring irrespective of the sensors and platforms used.

—we only focus in this section on the recently developed techniques that target any of the three functionalities during oil spill monitoring (detection, estimation, and classification) using non-satellite-based approaches.

Several drone-based techniques are recently suggested for oil spill monitoring. [53] presents thermal imaging methods and tools applied to simulated and lab-based experimental data to detect oil spills in seawater using drones. The simulation environment is made to be very similar to the Gulf of Mexico spill in 2010. The drone can be used in two operational modes: the first mode is when the spill incident is known, then the task is to locate it exactly. The second mode is when operating to look for potential spills and for nearby ships that caused them. After collecting thermal images using the thermal camera mounted on an unmanned aerial vehicle (UAV), the temperature profile of collected data is studied using image processing techniques. The proposed system shows the ability to draw a rectangular contour around the spill region but not the accurate contour. The thickness of the spill under test is not reported. Another drone-based solution equipped with a thermal camera is proposed in [54]. The system is suggested for industries, especially for the Bahrain Petroleum Company (Bapco), to inspect oil and gas leakages. It uses AI-based (decision tree (DT), random forest (RF), and support vector machine (SVM)) onboard processing to monitor oil pipelines for possible leakages and cracks. The training is done based on a real dataset of methane pipeline leakage detection provided by Bapco, Tatweer Petroleum, and the National Space Science Authority (NSSA). The proposed algorithms are accelerated on hardware using parallel processing to allow real-time alerting with less than 100 milliseconds delay. No results for oil spill leakage from pipelines are presented. The presented work is relying only on a single dataset while multiple datasets should be included. [55] also targets the first functionality of the monitoring system (detection) by presenting a UAV-based aerial solution to automatically identify the contour and localize oil spills. This approach is tested on simulated, experimental, and field data through simulated oil spills in the Leixoes Harbour and the Douro river in Porto in Portugal and in the Puerto de A Coruna in Spain. In [56], a deep-learning-based method is proposed to control marine oil pollution. It implements an SVM approach that processes visual camera images to identify oil-polluted areas. Afterward, it predicts the movement of the polluted area by calculating the optical flows. The algorithm is applied to the 2016 Tegent Cruises dataset in Shimen in northern Taiwan. The accuracy of the SVM classification varies between 85.71 and 99.95%. Another deep learning approach is suggested by [57]. It presents a CNN-based novel framework to detect small oil spills inside a port using a thermal infrared camera mounted on a drone. Three kinds of oil (HFO, DMA, and ULSFO) that are frequently used in the port of Antwerp are included during the experiment. A mean intersection over union (mIoU) of 89% is achieved. The proposed technique is functional within a 31.9 m by 42.1 m field of view and is useful for relatively small oil spills. [58] uses hyperspectral images to feed a one-dimensional convolutional neural network to identify the type of oil spills. Using the adaptive long-term moment estimation (ALTME) optimizer, the oil spill spectral information is learned. The experiment is conducted 20 m away from the Yellow Sea Shore in China, in the pool of Qingdao Scientific Research Base. The technique achieves a detection accuracy of more than 98.09% in detecting different predefined classes of oil films of thicknesses between 1 and 3.5 mm. To summarize, [53–57] all target spill detection (functionality #1), whereas [58] also targets the thickness estimation (functionality #2) in predefined classes (between 1 and 3.5 mm) and the oil type identification (functionality #3). This reinforces the need for our new proposed system that targets the three

different functionalities at the same time. Compared with the work presented in [58], the proposed new solution is using the wide-band radar sensor instead of a hyperspectral visual sensor (check differences in Section 2.1). Furthermore, the new approach uses maximum-likelihood algorithms on top of different machine learning algorithms to provide the results for monitoring. Also, the approach aims the thickness estimation up to 10 mm value, and it is feasible to be implemented on drones for onboard processing.

Other techniques, which are not drone-based, are also proposed in the literature for oil spill monitoring. [59] proposes an optical fiber surface plasmon resonance for oil spill detection and thickness estimation. At the water-oil and ail-oil interfaces, the sensor records an absolute sensitivity of 1.373%/mm and 2.742%/mm in the thickness ranges 0–5 mm and 0–10 mm, respectively. Although their approach can detect thicknesses in the 1–10 mm range, however, it requires in-situ sampling. [60] presents multiple machine learning algorithms (RF, SVM, DNN, and DNN with differential pooling) that process images from the high-resolution hyperspectral sensor to identify the oil type based on the reflectance spectra. Four types of oil are tested in this work, including crude oil, diesel, lubricant, and heavy diesel. The oil thickness and the wind conditions are not provided as inputs to the machine learning models to test their accuracy with the minimal amount of available information. All tested models can differentiate between heavy oils. But for light oils, RF fails to do the correct classification, while the neural network models provide better classification than the SVM. This technique is not remote-based and should be used after the detection of oil spills. [61] develops a novel microwave oil spill sensor to determine the thickness in the range of 10s mm using an ultra-wideband radar operating between 0.3 and 3000 MHz. The performance of the system is tested under static experimental conditions. When deploying the system in the sea, the impact of the waves should be considered.

A comparison between the functionalities provided by the developed techniques above and our new approach is presented in **Table 1**.

3. Drone-based radar approach

In this section, we describe in detail the proposed approach for oil spill monitoring for oil spill detection, estimation, and classification.

3.1 System model

3.1.1 Reflection coefficient for multi-layer structure

To physically model the oil slicks on top of the sea surface, we consider a multi-layer structure: air, oil, and seawater. We study the reflection of the electromagnetic waves from the sea layer covered by an oil layer, which is modeled as a thick slick with a thickness of up to 10 mm [13]. **Figure 1** shows such a simulated oil spill. When the ocean is calm and the wind speed is low, such a thick layer significantly reduces the surface roughness [37, 62], dampens capillary and short gravity waves, and calms the smaller waves on the sea [63]. As a result, within the radar cross section, the incident electromagnetic waves are reflected along the specular component due to the smooth surface. By operating the radar on a nadir-looking system, the reflected power is fully reflected for normal incident waves, without losses due to off-nadir backscattering.

Sensor(s)	Detection	Thickness Estimation	Classification	Notes	Reference
Thermal camera	Yes	No	No	Image processing	[53]
Thermal camera	Yes	No	No	AI-based techniques (DT, SVM, RF)	[54]
Visual/Thermal cameras, Lidar	Yes	No	No		[55]
Visual camera	Yes	No	No	SVM Prediction of track	[56]
Thermal infrared	Yes	No	No		[57]
Hyperspectral sensor	Yes	Yes [1–3.5 mm]	Yes	Post Processing	[58]
Fiber-Optic Surface Plasmon Resonance	Yes	Yes [0–10 mm]	No	Not drone-based, using in-situ sampling	[59]
Hyperspectral sensor	No	No	Yes	Not drone-based, using RF, SVM, and DNN	[60]
Ultra-wideband radar	No	Yes [10s of mm]	No	Not drone-based, under static conditions	[61]
Wideband Radar	Yes	Yes [0–10 mm]	Yes	Onboard processing	Proposed solution

Table 1.
Non-satellite-based state-of-the-art techniques for oil spill monitoring.
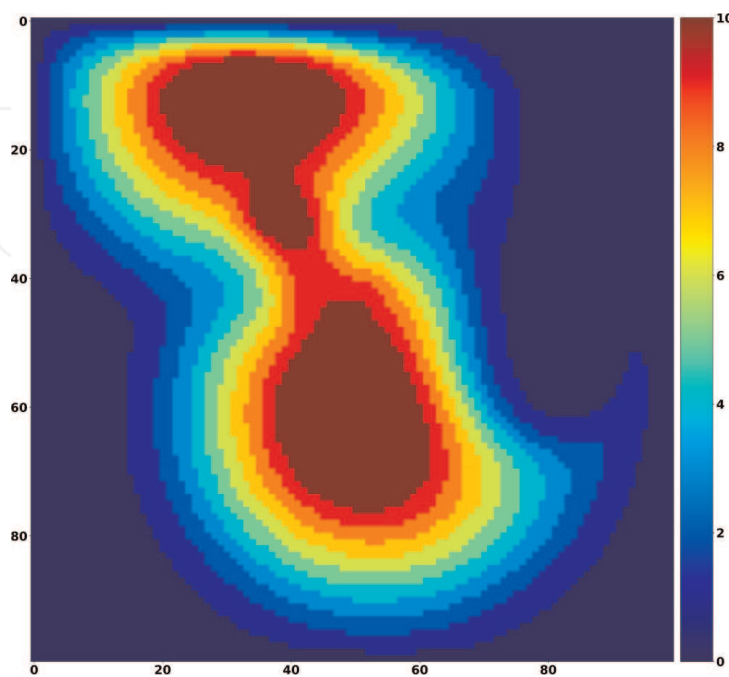
Figure 1.
Simulated oil spill with thickness range from 0 to 10 mm.

We define the electrical properties (relative dielectric constants) for the air, oil, and seawater to be respectively ε_1, ε_2, and ε_3. The different media are assumed to be non-magnetic. If radar reflections from the seafloor are neglected, we can calculate the field reflection coefficients for the layers at the boundaries where interaction with electromagnetic waves occurs. They are denoted for the first interface (between air and oil) and the second interface (between oil and water) by ρ_{12} and ρ_{23}, respectively. Hence, the power reflection coefficient for the three-layer structure, also denoted by the reflectivity R, is derived using the Transfer Matrix Approach [64, 65] as:

$$R = \left| \frac{\rho_{12}e^{j\delta} + \rho_{23}e^{-j\delta}}{e^{j\delta} + \rho_{12}\rho_{23}e^{-j\delta}} \right|^2 \tag{1}$$

δ is the propagation constant that is dependent on the oil's relative permittivity (ε_2), the frequency of the electromagnetic wave (the wavelength λ), and the thickness of the oil layer (d). It is given by:

$$\delta = \frac{2\pi \sqrt{\varepsilon_2}\, d}{\lambda} \tag{2}$$

3.1.2 Smooth and rough surfaces

Several statistical attributes can be calculated for a random surface [66]. The surface height measurements may be described using standard statistical parameters, namely:

- the height standard deviation (s), which is also called the rms-height

- the surface correlation length that measures the degree of correlation between the surface at different locations

Based on the surface statistics with respect to the electromagnetic wavelength, we can differentiate between two types of surfaces: a perfectly *smooth* (flat) or *rough* surface. If the correlation length of the ocean waves is large and the rms-height of capillary waves is very small, as it is for calm ocean conditions, then the surface is considered smooth. In this case, radar reflections are along the specular direction and can be calculated according to Eq. (1). Otherwise, a non-coherent component is introduced in the scattering pattern along all directions other than the specular, whenever the surface is rough. For this, with θ denoting the incident angle of the electromagnetic waves to the interfaces, the reflectivity in the specular direction is called the coherent reflectivity $R_{coherent}$, and it is given by:

$$R_{coherent} = R.e^{-4\left(\frac{2\pi\, s\, \cos(\theta)}{\lambda}\right)^2} \tag{3}$$

### 3.1.3 Reflectivity behavior

For our approach, we suggest the incorporation of multiple bands using remote sensing nadir-looking wide-band radar sensors. Since frequencies from the L-band (1–2 GHz) will not change the reflectivity value over the 1–10 mm thickness range by more than 1 dB, they are not considered to be relevant for the proposed approach. Instead, we will use frequencies from the C-band (4–8 GHz) and X-band (8–12 GHz).

To better understand the reflectivity behavior at each wave frequency, **Figure 2** shows the reflectivity value defined in Eq. (1) versus the oil thickness, which is varied from 1 mm to 10 mm where different subplots correspond to different scanning frequencies at increments of 1 GHz from 4 to 12 GHz [67]. The relative dielectric constant of the air and thick oil is 1 and 3, respectively. We neglect the imaginary part of the relative permittivity of the oil, which is of order 0.01 [68]. The relative dielectric constant of seawater depends on the water temperature (assumed to be 20 degrees), the water salinity (assumed to be 35 ppt), and the frequency of the radar signal [66]. For ease of reference, we also mark the mean reflectivity value in the case of no oil spill as a constant straight line per subplot.

For instance, at 4 GHz, the curve of the reflectivity is monotonically decreasing slowly with the thickness. It has a very small slope at small thickness values (0–3 mm), but this slope increases with the increase of the oil slick thickness (3–7 mm). At some thicknesses, any error in the power reflectivity measurements at 4 GHz would mislead the oil detection due to the very small variation from the water reflectivities. In addition, for small thickness values, the difference between reflectivity values is very small, so the estimation could go easily wrong. A different pattern is observed at higher frequencies (7–12 GHz). The reflectivity curve admits a steeper slope for small values of thicknesses, which improves the detection of oil slick thickness. However, due to the appearing cyclic behavior, many thickness values give the same reflectivity value leading to false interpretations for detection or estimation. Therefore, it is important to use more than one frequency to improve the detection or estimation. To see the effect of the relative permittivity of the oil on the reflectivity, **Figure 3** studies the variation of this parameter evaluated at two frequencies: 4 and 12 GHz [69]. For the same frequency, the effect of the variation in the relative permittivity on the reflectivity value is dependent on the oil thickness. Also, by
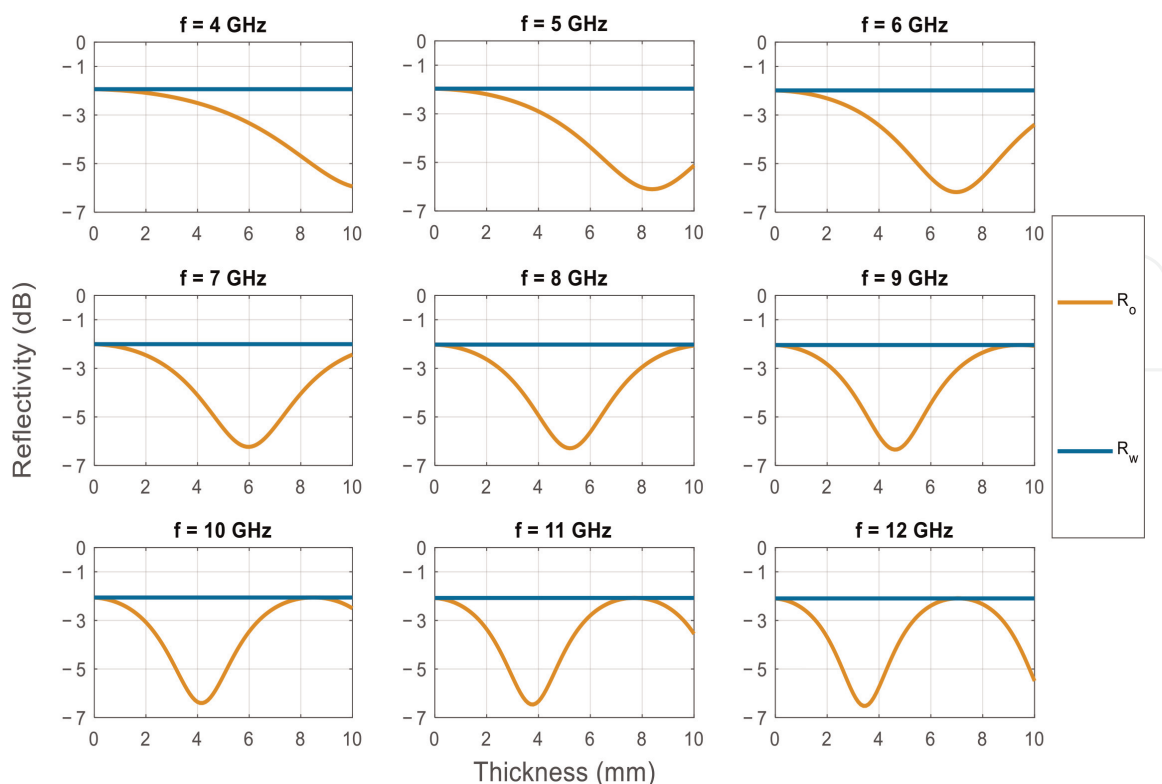
Figure 2.
Reflectivity (in dB) versus oil slick thickness (in mm) at different scanning frequencies. Retrieved from [67].
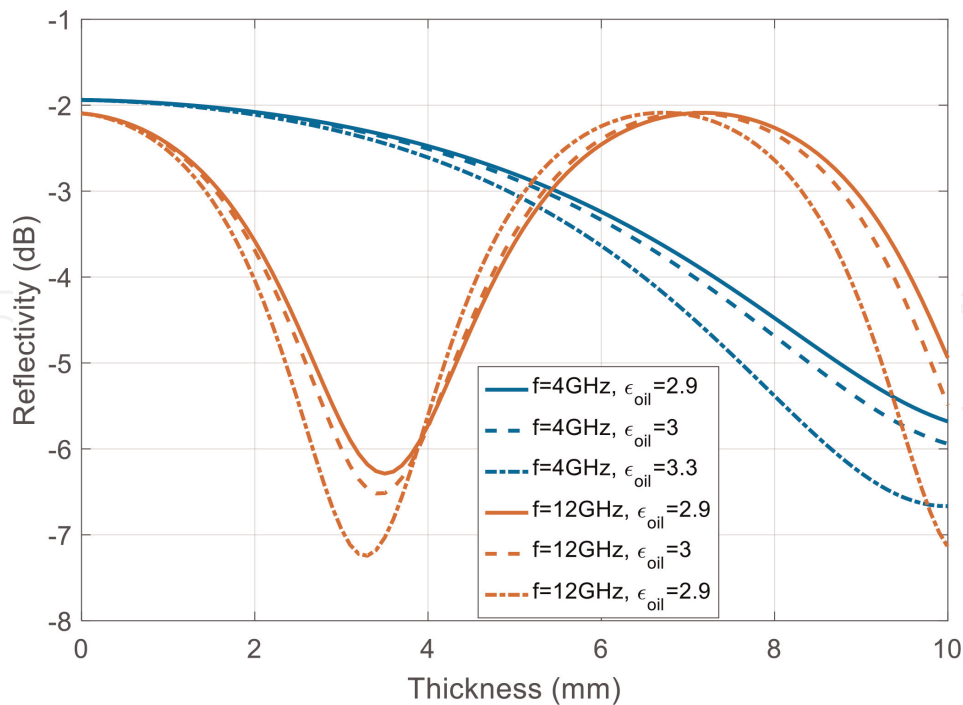
Figure 3.
Reflectivity R (in dB) versus oil thickness (in mm) at different frequencies (4 GHz, and 12 GHz) and different oil dielectric constants. Retrieved from [69].

looking at the reflectivity plots at the same frequency, they look very similar over the full thickness range even if the relative permittivity of the oil slick is changing. However, the reflectivity behavior varies a lot from one frequency to another.

3.2 Detection

To perform the detection functionality of the monitoring system, we are proposing in this section different detection algorithms that use the statistical characterization of the reflectivity values and their distribution under different oil thicknesses to obtain a final decision on whether oil exists or not. Any previous knowledge about the existence or absence of oil in the surface scanned should be taken into consideration to weigh the probability of the decision in the detector block. Nevertheless, without any previous knowledge about the spill situation, the detector decision will be totally based on the statistics of the measured power reflection coefficients ratio [69].

Let "o, w" be the events indicating the presence of the oil slick and the water, respectively. Let R be the event representing the measurement of the reflectivity value (s). R could represent one or more reflectivity values that are measured at the same or at different frequencies. The reflectivity values are assumed to be independent events, i.e., they are uncorrelated in the time domain at multiple observations, and in the frequency domain at multiple frequency measurements. After some derivation steps shown in [69], the detector algorithm evaluates the following ratio:

$$\frac{\Pr(o|R)}{\Pr(w|R)} = \frac{\Pr(R|o)}{\Pr(R|w)} \underset{<_w}{\overset{>^o}{}} 1 \qquad (4)$$

With this ratio, the detector compares the probability of getting an oil or water event given that radar reflectivities are measured. If the ratio gives a result greater

than unity, the decision indicates the oil's existence. Otherwise, the decision indicates that the seawater surface is clean. We note that the probability of obtaining a measured reflectivity value given that the oil or water exists is evaluated using the corresponding probability density function (pdf). For this, we propose several algorithms for different detectors:

- *Single observation at multiple frequencies* [70]: a wide-band radar is used to scan a target scene once, and K measurements of reflectivity are sampled at K different frequencies.

- *Multiple observations at single frequency* [71]: a narrow-band radar scans a target scene multiple times. M measurements of reflectivity are made at the same frequency.

- *Multiple observations at multiple frequencies* [69]: a wide-band receiver scans a target scene M time, and the reflectivity is sampled per scan at K different frequencies. M*K measurements of reflectivity are collected in total.

- *Joint-probability density function* [72]: the thickness of the oil slick is modeled as a random variable (RV) with an estimate of its probability density function. The algorithm is using the joint-pdf to calculate the probability of each event. Also, for this, a wide-band receiver scans a target scene M times, and the reflectivity is sampled per scan at K different frequencies.

Figure 4 shows the performance of dual-frequency detectors. For clarity, we also show the performance of the detectors running each of the two scanning frequencies separately. Evidently, the dual-frequency detectors outperform the single-frequency
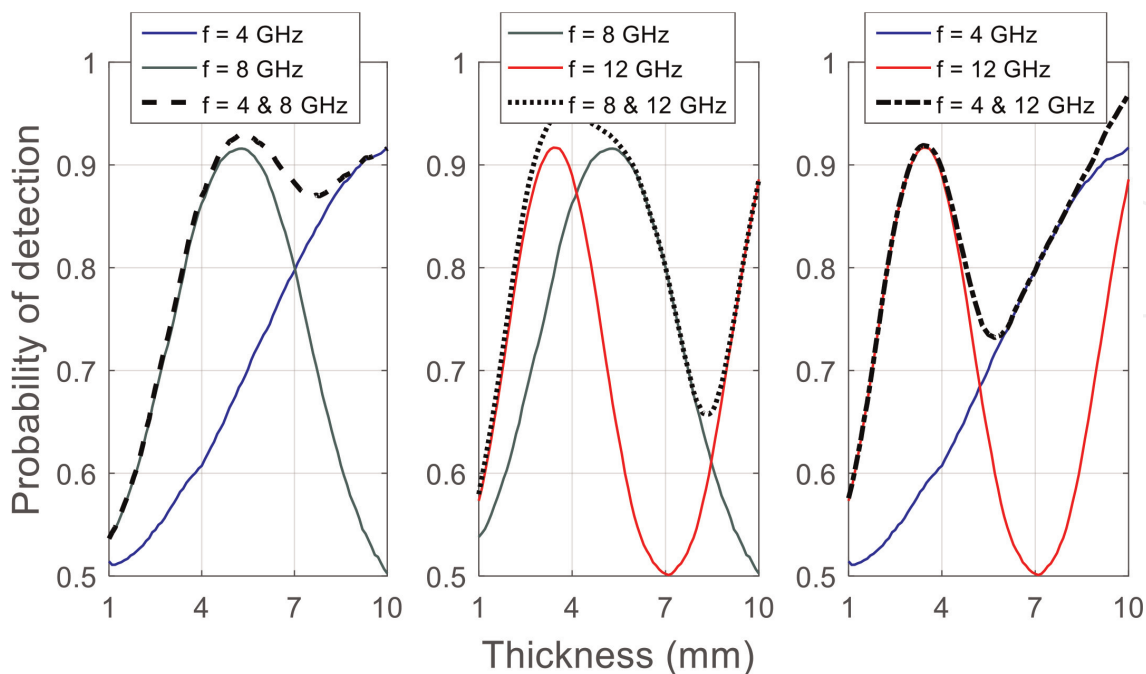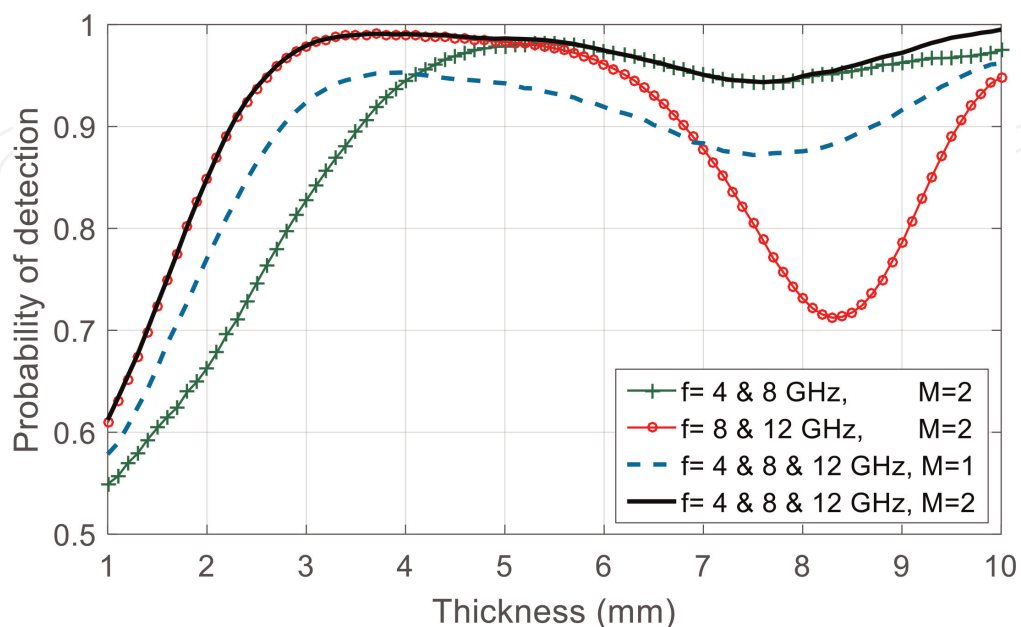

Figure 4.
Comparison between the probability of detection and the oil thickness (in mm) for different detector algorithms: Single-frequency detectors at 4 GHz, 8 GHz, and 12 GHz, and dual-frequency detectors using combinations of these frequencies.

detectors. At thickness values where the accuracy of a single-frequency detector is low, the dual-frequency detector gives more weight to the decision of the pair detector. For instance, a 12 GHz detector performs poorly for d = 7.2 mm because it has the same reflectivity value as the water (refer to **Figure 2**). However, the (4 GHz, 12GHz) detector optimally tracks the performance of a 4 GHz detector.

Although dual-frequency detectors are better than single-frequency detectors, there are still some thickness ranges where the probability of detection is affected by the ambiguity points. To boost the performance of the detection, we increase the number of frequencies K and observations M. Results in **Figure 5** show that a higher probability of detection is further obtained over the full range of thicknesses. Using three frequencies (4 GHz, 8 GHz, 12 GHz) and two scans (M = 2) of the target scene, the detection accuracy is above 90% for all thickness values above 3 mm. Additional scans would further be required to improve the probability of detection of thin oil slicks. Fortunately, performance requirements are less strict for small thickness values. By comparing the performance of the tri-frequency detector with single observation to the dual-frequency detectors with double observations, we notice that the first detector is better since it provides a very high percentage of correctness at the large thickness values (i.e., cases where oil detection is crucial) and very good behavior at small thickness values, which are more challenging for oil detection but less severe in false alarm scenarios. Additionally, the performance of the detectors is studied under a blind detection scenario in which the scanning of the scene is done without any knowledge about the exact or the estimated thicknesses of spilled oil. This type of detection is based on the joint-pdf that takes into consideration all the possible thicknesses with their probabilities in order to weigh the final decision. The distribution of oil thickness is assumed to be uniform over the range (0–10 mm). Results show the same behavior as detailed in [72]. The detector can provide correct decisions in different thickness ranges at different frequencies. The probability of error can be decreased by using dual- and tri-frequency detectors. Additional error can be

Figure 5.
Comparison between the probability of detection and the oil thickness (in mm) for different detector algorithms: Dual-frequency detectors and multi-frequency detectors, using single (M = 1) and double observations (M = 2).

compensated by using more scans. However, in the range where the oil thickness is small (< 2 mm), the probability of detection does not exceed 65% indicating low certainty.

Previous results are obtained under the assumption that the surface is smooth due to very low wind speeds and calm ocean conditions. For higher wind speeds and rms-height of the seawater, the surface roughness increases. We present the performance of the detectors for different roughness scenarios in detail in [69]. Results show that the performance overall is reduced.

3.3 Estimation

In this section, we complement the detection of oil spills (functionality #1) with a new approach targeting the estimation of the oil slick thickness (functionality #2). We present Maximum Likelihood single-, dual-, and multi-frequency estimators. The reflectivity values evaluated at one, two, or multiple frequencies over all possible thickness values form the constellation set that is used for the estimation. The estimator uses the Minimum-Euclidean distance algorithm, in predefined 1-D, 2-D, or K-D constellation sets, on radar reflectivities to estimate the thickness of the oil slick. Every constellation set is divided into different mapping regions that are bounded optimally between all the theoretical reflectivity values constituting the constellation. Any reflectivity value R obtained in one region is mapped by the estimator to the thickness that provides theoretically the nearest reflectivity value.

The derived algorithms are the following:

- *1-D estimator* [73]: It is a single-frequency estimator. The probability of error is minimized by choosing the thickness, which minimizes the Minimum-Euclidean distance between the measured reflectivity R and all possible calculated reflectivities constituting the constellation set. For the single-frequency estimator, the constellation set is in a single dimension.

- *2-D estimator* [73]: The dual-frequency estimator uses two reflectivity values in the constellation set spanning two dimensions.

- *2-D estimator iterative approach with multiple observations* [74]: The presented algorithm uses optimized predefined 2-D constellation sets by utilizing the best pair of frequencies for each possible thickness value. Then, it processes sequentially the separate estimations done to optimize the estimation procedure.

- *K-D estimator* [67]: Using K-frequencies in the estimation, the constellation set will span K dimensions. When using M observations that are uncorrelated in time, we do the averaging of the measured reflectivity values in K-dimension at each frequency of measurement.

- *SVM approach* [75]: A support vector regression that is following a supervised learning approach and is trained on reflectivities calculated for three radio-wave frequencies is proposed to predict oil thicknesses between 1 and 10 mm.

- *ANN approach* [76]: An artificial neural network that processes reflectivities evaluated at nine radio-wave frequencies is proposed to predict oil thicknesses between 1 and 10 mm.

Using a single-frequency estimator in C-band (4–8 GHz), the mapping regions at low thickness values will be close to each other as shown in detail in [67, 73]. A small noise power may shift the reflectivity values from one region to another. If so, this will be considered an error in the estimation process. At higher frequency values in X-band (8–12 GHz), many thickness values will give the same reflectivity due to its cyclic behavior. Therefore, even in an ideal case when no noise is introduced during the measurements, the estimator is not capable to provide a correct estimation. *This highlights the need to use the combination of reflectivity measurements (2-D or 3-D estimators) to achieve accurate thickness estimation.* Using dual- and tri-frequency estimators, one question will rise: which combination of frequencies is to be used? The best frequency pairs and triads, for each possible thickness between 1 and 10 mm, are derived in [74, 67] respectively. [74] also proposes an advanced iterative procedure to use the 2D estimator for accurate and reliable thickness estimations.

Figure 6 shows the histograms of the thicknesses estimated by K-D estimators when the actual thickness d is 5 mm with single and multiple (M = 3) scans. The single-frequency (1-D) estimator uses f_1 = 4 GHz, and f_2 = 12 GHz. The dual-frequency (2-D) estimator uses both f_1 and f_2. The 3-D estimator uses an additional frequency f_3 = 7 GHz. The 4-D estimator uses f_1, f_2, f_3 in addition to f_4 = 10 GHz. The 2-D estimator with three scans still provides thickness values from all possible values. The 4-D estimator with three scans decreases the error in the estimation to 4 mm with a probability of correctness of 80%. The percentage error obtained by all estimators under different scenarios is presented in **Table 2**. To check the distribution of the histograms of errors in estimation, refer to Appendix A in [67].
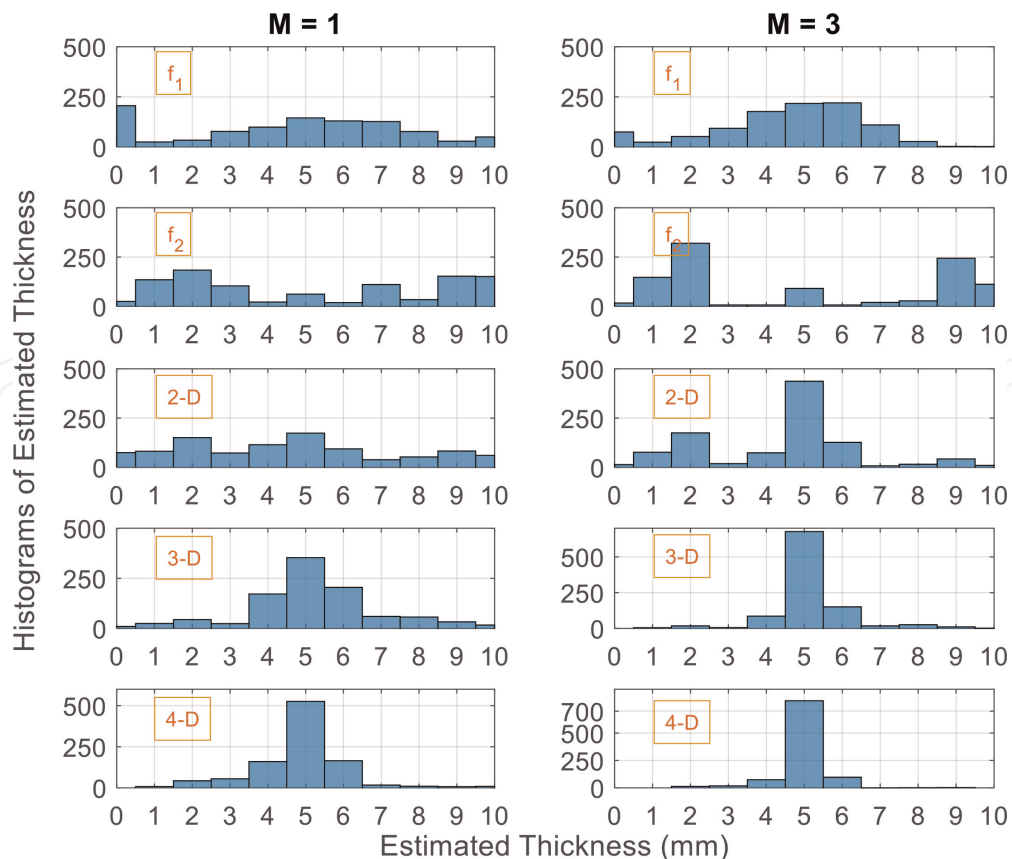
Figure 6.
Histograms of the thicknesses estimated by 1-D, 2-D, 3-D, and 4-D estimators with single and multiple scans M = 3. The actual thickness d is 5 mm. Retrieved from [67].

Probability of error (%)	M	f_1	f_2	2-D	3-D	4-D
d = 10 mm	1	46	78	35	32	30
	3	42	63	14	13	11
d = 5 mm	1	85	94	83	65	47
	3	77	91	58	33	20
d = 1 mm	1	97	85	83	77	72
	3	94	75	65	56	49
	10	90	58	36	32	26
	50	79	41	10	9	6

Table 2.
Percentage error obtained by different estimators for different slick thicknesses. Adapted from [67].

Although some estimators provide a good probability of correctness, it is not sufficient to have a definite decision. We should rather look at the error distribution in the estimation to ensure that the estimations are reliable. Therefore, we should always increase the number of frequencies or scans done to make sure that good and enough estimation information is provided.

We developed an experimental setup to collect radar reflectivity measurements from an oil-spill lab experiment with calm water surface conditions for very low wind speeds with no wave action. The experimental setup includes details about the system model with the multi-layer structure, the radar calibration technique, and other setup parameters [77, 78]. We applied the estimation algorithm to these experimental values. **Figure 7** shows the histograms of estimated thicknesses by 1D, 2D, 3D, and 4D estimators based on experimental reflectivity values with a single scan (M = 1), when the actual thickness is 3 mm. As expected, 1D estimators using a single frequency are not providing very good results. Using f1, the highest estimations are for 4 mm, the probability of error is 72%, and the maximum deviation from the correct value is 7 mm. Using f2, the deviation is decreased to 1 mm with a probability of error of 47%. However, single-frequency estimators are never used alone, therefore, including f2 in the 2D estimator again increases the probability of error to 68% but provides the advantage of decreasing the maximum deviation to 1 mm. For the higher-order 3D estimator, the probability of error decreases to 28% with the same maximum deviation. For the 4D estimator, the performance is further improved, and the probability of error is reduced to 6%. Thus, the results shown validate the proposed higher-order estimators on in-lab experimental data.

Another proposed estimation algorithm is based on a machine learning approach [75]. For this, a support vector regression (SVR) model that is following a supervised learning approach is trained on reflectivities calculated for three radio-wave frequencies to predict oil thicknesses between 1 and 10 mm. The input features to the SVR model are the power reflection coefficients (reflectivities) evaluated at $f_1 = 4.39$ GHz, $f_2 = 6.98$ GHz, and $f_3 = 9.07$ GHz. After training the model using 80% of the simulated data, it is validated on the remaining 20% of the simulated and on in-lab experimental data. The model yielded an R^2 score of 0.992 on the simulated data, which is very close to 1 indicating that the regression predictions are very close to the actual oil thicknesses. The model is supposed to predict a continuous value of the thickness as the predicted output. But by rounding the estimated thickness to the closest integer, we
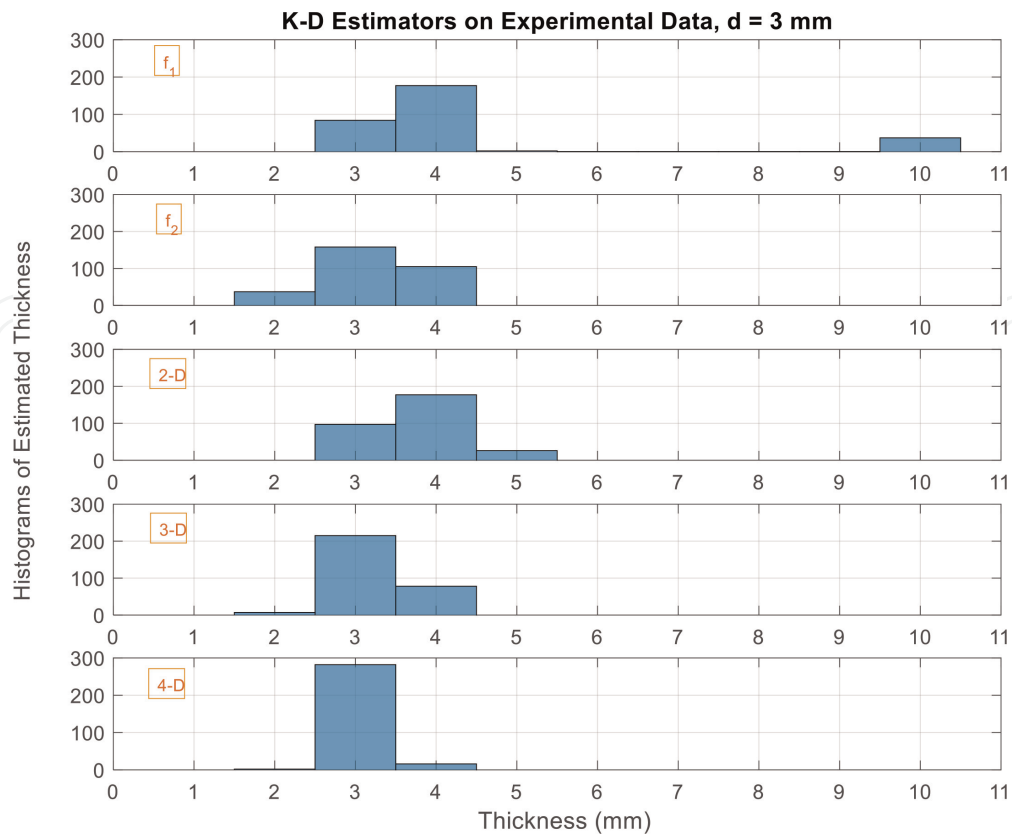
Figure 7.
Histograms of the thicknesses estimated by 1D, 2D, 3D, and 4D estimators based on experimental data with single scan M = 1. The actual thickness is 3 mm. Retrieved from [67].

get the following percentages of estimating the correct value in the confusion matrix: [62.4, 95.5, 99.7, 97.7, 97.7, 99.6, 99.4, 95.4, 80.5, 89.6%] for the thicknesses [1, 2, 3, 4, 5, 6, 7, 8, 9, 10 mm] respectively. The R^2 score obtained on the experimental data is 0.86 indicating that the experimental thickness values and the predicted thicknesses are close even though the model is only trained on simulated data and is not exposed to any experimental reflectivity. For further validation, even though the model is trained on calm surface data, it is tested with rough surfaces in two scenarios for slick thicknesses: 5 mm and 8 mm. The model's predictions are mostly concentrated at 6 mm for the 5 mm spill. Similarly, for the 8 mm spill, the predictions are mostly at 7 and 8 mm. This shows that using a machine learning algorithm for oil thickness estimation is an attractive approach. Another algorithm is developed in [76], but for convenience, we will discuss it in the following section. This concept can be further developed by using larger and more complex machine learning models and more diversified training data to achieve better thickness estimations in varied environments.

3.4 Classification

An important task to perform during oil spills is to specify the oil type to predict the environmental damage to maritime life. The oil type classification could be qualitatively similar to what is proposed by [60, 79–81]. Another way for classification is by analyzing the physical characteristics of the oil material, namely the relative dielectric constant, as we proposed in [76]. In this work, we use an artificial neural network (ANN)-based model to estimate the relative permittivity of oil slicks for

different oil-types classification. In addition, the model can predict the thicknesses of such oil slicks at the same time. The input features to the model are nine radar reflectivity values measured simultaneously and selected uniformly from C- (4–8 GHz) and X- (8–12 GHz) bands. The ANN-model post-process these measurements to extract the implicit information about the thickness and the relative permittivity of the thick oil layer covering the sea surface, even though the reflectivities and the estimated parameters have a highly nonlinear relationship. To further improve the model's accuracy, we also incorporate multiple observations to boost the estimator's performance. Results show that by jointly analyzing the reflectivity behavior at multiple frequencies, the model explores their dependence over the full plausible range of thicknesses. The predicted thicknesses are accurate to +/− 0.5 mm in most cases. For example, testing the model at 5.5 mm would still lead to estimations between 5 and 6.1 mm. Similarly, relative permittivity values 2.9, 3, and 3.1 are approximated accurately where the shift in estimations' mean is smaller than 0.05. The error in estimations for the remaining values 2.8, 3.2, and 3.3 is higher. To test the performance of the model, we simulate an oil spill scenario when the thickness of the oil slick that is close to the source is 10 mm, and it decreases gradually going away from the source to 1 mm. The trained ANN model shows that it can perfectly reconstruct the spill environment with accurate estimations of the thicknesses and the relative permittivity, where the error of the average estimate for the latter over the full map is 3% only. To further validate the performance of the model, it is applied to in-lab experimental data when the actual thickness is 7 mm. After collecting 13 measurements, the estimated thickness is 7.65 mm compared with 8.2 with a single scan measurement. Unfortunately, we are not able to compare the estimated permittivity with the actual value since the latter has not been measured during the in-lab experimental procedure.

3.5 Onboard processing

Our proposed approach targets the implementation of the monitoring functionalities on board, instead of collecting measurements from the site and post-processing them offline afterward. This will ease the monitoring and most importantly will allow the quick assessment of the spill area, to take the best measures and actions toward the possible damage. For this reason, it is very important to check the feasibility of implementing the proposed approach onboard, especially since the platform that we are suggesting is the drone, which is a battery-powered device where the energy and power consumption are of high importance. We show the feasibility of our approach for onboard processing by selecting one of the previously described algorithms and implementing it on a hardware platform, namely the Pynq Z1 Field Programmable Gate Array (FPGA). While machine learning algorithms are often considered high-power consuming and introduce a high complexity in terms of memory footprint and computational requirements, we select the ANN model that performs the estimation and classification functionalities for the implementation. It is also good to note that including "0 mm" as one class for the regression estimation is equivalent to including the detection functionality. Therefore, we believe that the implementation complexity of this model is very significant since the latter can perform all the main required functionalities for oil-spill monitoring at the same time. Results show that, based on the architecture used during the implementation, only 1.13–28.37% of the available resources are utilized by the network. Similarly, the power consumption varies between 34 and 133 mW, which is negligible compared with the power drawn by

drones in the order of 10th of watts. This verifies the feasibility of our ANN-based approach and demonstrates the suitability for a practical scenario.

3.6 The proposed system: Complementary solution

For completeness of the system-level analysis, we suggest having a complete system composed of four subsystems as shown in **Figure 8**:

1. Drone: It is the part used for tactical response. Whenever there is a flag raised for possible oil spills (by witnesses or due to accidents), multiple drones that mount nadir-looking wide-band radar sensors are sent to place. Measurements at different frequencies are collected. Based on the weather conditions and the ocean's waves, multiple scans could be used to improve the accuracy of the results. The measurements are then processed onboard using the proposed algorithms to provide an initial assessment with respect to the detection, estimation, and classification functionalities.

   a. The detection algorithms proposed in Section 3.2 are applied. If the probability of detection exceeds the threshold set by the persons in charge, then there is a need to prepare to start the contingency plan.

   b. The estimation algorithms proposed in Section 3.3 are applied. Thickness values greater than 1 mm indicate the need for quick intervention because the oil slick will persist for a long period of time.

   c. The classification algorithm in Section 3.4 is applied to have an indication about the oil type.
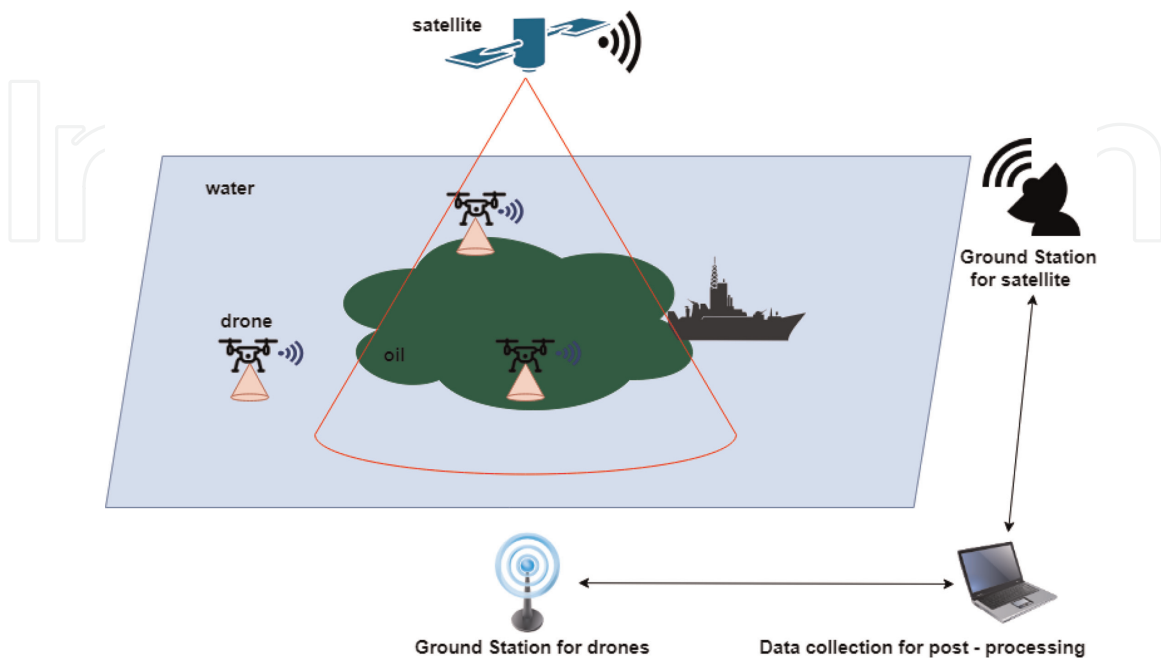
Figure 8.
System-level view of the oil spill monitoring system.

  d. The results are sent to a ground station to combine results from different drones and locations on the corresponding map.

2. Satellite: It is the part that can provide the synoptic view of the oil spill scene. After the confirmation of the spill based on the initial assessment, the satellites are used to provide the synoptic view and to get a better estimate of how the spill is displaced over time. The satellites are supposed to transmit SAR images to corresponding ground stations.

3. Data collection center: It is the part responsible for data collection, analysis, and making decisions. SAR images are analyzed and compared with results received from drones. Corresponding measures are taken, and the oil spill contingency plan is launched. Oil spills are then tracked over time.

4. Conclusion

This work shows that by processing radar power reflectivity values, taken from nadir-looking systems under weather conditions suitable for cleaning operations, thick oil slick thicknesses up to 10 mm can be detected, estimated, and classified. The accuracy of each function is dependent on the selected statistical algorithm. This approach is novel since it provides most of the information that is required for an effective contingency plan at the same time during the early stage of the spill. In addition, this novel approach being implemented on drone platforms is a suitable system for tactical responses needed during contingency plans. Moreover, the new approach aims to complement state-of-the-art techniques, such as satellite-based SAR, by covering calm ocean conditions and low wind speeds scenarios that challenge other techniques for oil spill monitoring. Maximum-likelihood and machine learning statistical algorithms could be used directly to quickly assess the scene. The ANN model shows very low complexity, low power consumption, and high accuracy. This demonstrates the feasibility to apply the approach for onboard processing. Despite all the advancement that is presented, there are still open questions, tasks, and challenges to consider in this field for utilized practical solutions. A further investigation on the algorithmic level is still required to make sure that the performance will not decrease given the variable dynamics that could be introduced in the physical environment. Also, the complexity of all proposed approaches should be studied to check the feasibility of implementing them on hardware platforms for onboard processing. Despite the need for detection, thickness estimation, and classification, tracking the spill is also very important on a small scale, especially for moderate wind speeds. It would be useful to add this functionality as a capability of the drone-based solution by considering the weather conditions and the ocean state to track the spill over time. Finally, the proposed work is a proof of concept and helps take the oil-spill-related research work one step forward toward the development of operational tools for oil-spill intervention.

Conflict of interest

The authors declare no conflict of interest.

Notes/thanks/other declarations

Author details

Bilal Hammoud* and Norbert Wehn
Microelectronic Systems Design Research Group (EMS), Technical University of Kaiserslautern, Kaiserslautern, Germany

*Address all correspondence to: hammoud@eit.uni-kl.de

IntechOpen

References

[1] Jha MN, Levy J, Gao Y. Advances in remote sensing for oil spill disaster management: State-of-the-art sensors technology for oil spill surveillance. Sensors. 2008;**8**(1):236-255

[2] Fingas M. The Basics of Oil Spill Cleanup. Boca Raton, FL, USA: CRC press; 2002

[3] Grüner K, Reuter R, Smid H. A new sensor system for airborne measurements of maritime pollution and of hydrographic parameters. GeoJournal. 1991;**24**(1):103-117

[4] Oil Pollution Monitoring. Remote Sensing Exploitation Division. ESRIN—European Space Agency (ESA). p. 2. Available online: http://www.esa.int/esapub/br/br128/br128_1.pdf. [Accessed: December 18, 2018]

[5] Ipingbemi O. Socio-economic implications and environmental effects of oil spillage in some communities in the Niger delta. Journal of Integrative Environmental Sciences. 2009;**6**(1):7-23

[6] Sandifer PA, Ferguson A, Finucane ML, Partyka M, Solo-Gabriele HM, Walker AH, et al. Human health and socioeconomic effects of the Deepwater horizon oil spill in the Gulf of Mexico. Oceanography. 2021;**34**(1): 174-191

[7] Svejkovsky J, Hess M, Muskat J, Nedwed TJ, McCall J, Garcia O. Characterization of surface oil thickness distribution patterns observed during the Deepwater horizon (MC-252) oil spill with aerial and satellite remote sensing. Marine Pollution Bulletin. 2016;**110**(1): 162-176

[8] Belore R, Trudel K, Morrison J. Weathering, emulsification, and chemical dispersibility of Mississippi canyon 252 crude oil: Field and laboratory studies. In: International Oil Spill Conference Proceedings (IOSC), Tampa, FL, USA. Washington, DC, USA: American Petroleum Institute; 2011

[9] Brekke C, Solberg AH. Oil spill detection by satellite remote sensing. Remote sensing of environment. 2005; **95**(1):1-3

[10] ITOPF, Oil Tanker Spill Statistics 2021, Available online: https://www.itopf.org/knowledge-resources/data-statistics/statistics/. [Accessed: August 1, 2022]

[11] Fingas M. Introduction to oil spills and their clean-up. In: Petrodiesel Fuels. Boca Raton, FL, USA: CRC Press; 2021. pp. 875-889

[12] Leifer I, Lehr WJ, Simecek-Beatty D, Bradley E, Clark R, Dennison P, et al. State of the art satellite and airborne marine oil spill remote sensing: Application to the BP Deepwater horizon oil spill. Remote Sensing of Environment. 2012;**124**:185-209

[13] Fingas M, Brown CE. A review of oil spill remote sensing. Sensors. 2017;**18**(1): 91

[14] Fingas M. The challenges of remotely measuring oil slick thickness. Remote Sensing. 2018;**10**(2):319

[15] Wang M, Hu C. Extracting oil slick features from VIIRS nighttime imagery using a Gaussian filter and morphological constraints. IEEE Geoscience and Remote Sensing Letters. 2015;**12**(10):2051-2055

[16] Goodman R. Overview and future trends in oil spill remote sensing. Spill

Science & Technology Bulletin. 1994;
1(1):11-21

[17] Fingas MF, Brown CE. Review of oil spill remote sensing. Spill Science & Technology Bulletin. 1997;**4**(4):199-208

[18] Fingas MF, Brown CE. An update on oil spill remote sensors. In: Proc. 28th Arctic and Marine Oil Spill Program (AMOP). Vol. 9. Canada: Tech. Seminar Calgary; 2005. pp. 825-860

[19] Samberg A. Advanced oil pollution detection using an airborne hyperspectral lidar technology. In: Laser Radar Technology and Applications X. Vol. 5791. Bellingham, Washington, USA: SPIE; 2005. pp. 308-317

[20] Salisbury JW, D'aria DM, Sabins FF Jr. Thermal infrared remote sensing of crude oil slicks. Remote Sensing of Environment. 1993;**45**(2):225-231

[21] Shih WC, Andrews AB. Infrared contrast of crude-oil-covered water surfaces. Optics Letters. 2008;**33**(24): 3019-3021

[22] Byfield V, Boxall SR. Thickness estimates and classification of surface oil using passive sensing at visible and near-infrared wavelengths. In: IEEE 1999 International Geoscience and Remote Sensing Symposium. IGARSS'99 (Cat. No. 99CH36293). Vol. 3. Piscataway, NJ, USA: IEEE; 1999. pp. 1475-1477

[23] Chen P, Li Y, Lan G, Liu B, Zhou H. Oil spills detection and monitoring using Airborn thermal infrared remote sensing in Dalian Xingang oil pipeline explosion. In: 2012 2nd International Conference on Remote Sensing, Environment and Transportation Engineering. Piscataway, NJ, USA: IEEE; 2012. pp. 1-4

[24] Ying L, Guo-xin L, Ji-jun L, Long M. Potential analysis of maritime oil spill monitoring based on MODIS thermal infrared data. In: 2009 IEEE International Geoscience and Remote Sensing Symposium. Vol. 3. Piscataway, NJ, USA: IEEE; 2009. pp. III-373

[25] Grimaldi CS, Coviello I, Lacava T, Pergola N, Tramutoli V. Near real time oil spill detection and monitoring using satellite optical data. In: 2009 IEEE International Geoscience and Remote Sensing Symposium. Vol. 4. Piscataway, NJ, USA: IEEE; 2009. pp. IV-709

[26] Huang H, Wang C, Zhang D, Zhan S, Hong S, Wang X, et al. Combining adaptive thresholding and region filling for xylene spills detection from ultraviolet images. In: 2018 OCEANS-MTS/IEEE Kobe Techno-Oceans (OTO). Piscataway, NJ, USA: IEEE; 2018. pp. 1-6

[27] Desbiens L, Roy V, Gravel JF, Taillon Y. 2.5 W, narrow linewidth, 259.0 nm, ruggedized DUV fiber laser source for remote benzene detection. In 2019 Conference on Lasers and Electro-Optics Europe & European Quantum Electronics Conference (CLEO/Europe-EQEC). Piscataway, NJ, USA: IEEE; 2019. pp. 1-1

[28] Yin D, Huang X, Qian W, Huang X, Li Y, Feng Q. Airborne validation of a new-style ultraviolet push-broom camera for ocean oil spills pollution surveillance. In: Remote Sensing of the Ocean, Sea Ice, and Large Water Regions 2010. Vol. 7825. Bellingham, Washington, USA: SPIE; 2010. pp. 159-169

[29] Skou N, Toselli F, Wadsworth A. Passive radiometry and other remote sensing data interpretation for oil slick thickness assessment, in a experimental case. ESA SP (Print). 1983;**188**:211-216

[30] Skou N. Microwave radiometry for oil pollution monitoring, measurements, and

systems. IEEE Transactions on Geoscience and Remote Sensing. 1986;**3**:360-367

[31] Laaperi A. Microprocessor controlled microwave radiometer system for measuring the thickness of an oil slick. In: 1982 12th European Microwave Conference. Piscataway, NJ, USA: IEEE; 1982. pp. 89-93

[32] Molkov AA, Kapustin I, Ermoshkin AV, Ermakov SA. Remote sensing methods for measuring the thickness of oil/oil product films on the sea surface. Sovremennye problemy distantsionnogo zondirovaniya Zemli iz kosmosa. 2020;**17**(3):9-27

[33] Hollinger JP, Mennella RA. Oil spills: Measurements of their distributions and volumes by multifrequency microwave radiometry. Science. 1973;**181**(4094): 54-56

[34] Brown CE, Fingas MF, Hawkins R. Synthetic aperture radar sensors: Viable for marine oil spill response? In: Arctic and Marine OILSPILL Program Technical Seminar 2003. Vol. 1. Ottawa, Ontario, Canada: Environment Canada; 1999. pp. 299-310

[35] Klemas V. Tracking and monitoring oil slicks using remote sensing. In 2012 IEEE/ OES Baltic International Symposium (BALTIC). Piscataway, NJ, USA: IEEE; 2012. pp. 1-7

[36] Yang CS, Kim YS, Ouchi K, Na JH. Comparison with L-, C-, and X-band real SAR images and simulation SAR images of spilled oil on sea surface. In: 2009 IEEE International Geoscience and Remote Sensing Symposium. Vol. 4. Piscataway, NJ, USA: IEEE; 2009. pp. IV-673

[37] Skrunes S, Brekke C, Eltoft T. Oil spill characterization with multi-polarization C-and X-band SAR. In: 2012

IEEE International Geoscience and Remote Sensing Symposium. Piscataway, NJ, USA: IEEE; 2012. pp. 5117-5120

[38] Skrunes S, Brekke C, Eltoft T, Kudryavtsev V. Comparing near-coincident C-and X-band SAR acquisitions of marine oil spills. IEEE Transactions on Geoscience and Remote Sensing. 2014;**53**(4):1958-1975

[39] Marzialetti P, Laneve G. Oil spill monitoring on water surfaces by radar L, C and X band SAR imagery: A comparison of relevant characteristics. In: 2016 IEEE International Geoscience and Remote Sensing Symposium (IGARSS). Piscataway, NJ, USA: IEEE; 2016. pp. 7715-7717

[40] Collins MJ, Denbina M, Minchew B, Jones CE, Holt B. On the use of simulated airborne compact polarimetric SAR for characterizing oil–water mixing of the Deepwater horizon oil spill. IEEE Journal of Selected Topics in Applied Earth Observations and Remote Sensing. 2015; **8**(3):1062-1077

[41] Hensley S, Jones C, Lou Y. Prospects for operational use of airborne polarimetric SAR for disaster response and management. In: 2012 IEEE International Geoscience and Remote Sensing Symposium. Piscataway, NJ, USA: IEEE; 2012. pp. 103-106

[42] Laneve G, Luciani R. Developing a satellite optical sensor based automatic system for detecting and monitoring oil spills. In: 2015 IEEE 15th International Conference on Environment and Electrical Engineering (EEEIC). Piscataway, NJ, USA: IEEE; 2015. pp. 1653-1658

[43] Dan W, Jifeng S, Yongzhi Z, Pu Z. Application of the marine oil spill surveillance by satellite remote sensing.

In: 2009 International Conference on Environmental Science and Information Application Technology. Vol. 1. Piscataway, NJ, USA: IEEE; 2009. pp. 505-508

[44] Rocca F. Remote sensing from space for oil exploration. In: 2015 IEEE International Geoscience and Remote Sensing Symposium (IGARSS). Piscataway, NJ, USA: IEEE; 2015. pp. 2876-2879

[45] Minchew B, Jones CE, Holt B. Polarimetric analysis of backscatter from the Deepwater horizon oil spill using L-band synthetic aperture radar. IEEE Transactions on Geoscience and Remote Sensing. 2012;**50**(10):3812-3830

[46] Bayındır C, Frost JD, Barnes CF. Assessment and enhancement of Sar noncoherent change detection of sea-surface oil spills. IEEE Journal of Oceanic Engineering. 2017;**43**(1):211-220

[47] Xu L, Wong A, Clausi DA. An enhanced probabilistic posterior sampling approach for synthesizing Sar imagery with sea ice and oil spills. IEEE Geoscience and Remote Sensing Letters. 2016;**14**(2):188-192

[48] Brown CE, Fingas MF. New space-borne sensors for oil spill response. In: International Oil Spill Conference. Vol. 2001, No. 2. Washington, DC, USA: American Petroleum Institute; 2001. pp. 911-916

[49] Lecomte, E. En Fevrier 2017, des Drones vont Traquer la Pollution Maritime. 2017. Available online: https://www.sciencesetavenir.fr/high-tech/drones/en-fevrier-2017-des-drones-vont-traquer-lapollution-maritime_109732 [Accessed: January 1, 2017]

[50] Kirkos G, Zodiatis G, Loizides L, Ioannou M. Oil pollution in the waters of

Cyprus. Oil Pollution in the Mediterranean Sea: Part. 2017;**II**:229-245

[51] Barenboim GM, Borisov VM, Golosov VN, Saveca AY. New problems and opportunities of oil spill monitoring systems. Proceedings of the International Association of Hydrological Sciences. 2015;**366**:64-74

[52] Hook S, Batley G, Holloway M, Ross A, Irving P, editors. Oil Spill Monitoring Handbook. Clayton, Victoria: Csiro Publishing; 2016

[53] Saleem A, Al Maashri A, Eldirdiry O, Ghommam J, Bourdoucen H, Al-Kamzari A, et al. Detection of oil spill pollution in seawater using drones: Simulation & lab-based experimental study. In: 2021 IEEE International IOT, Electronics and Mechatronics Conference (IEMTRONICS). Piscataway, NJ, USA: IEEE; 2021. pp. 1-5

[54] Alharam A, Almansoori E, Elmadeny W, Alnoiami H. Real time AI-based pipeline inspection using drone for oil and gas industries in Bahrain. In: 2020 International Conference on Innovation and Intelligence for Informatics, Computing and Technologies (3ICT). Piscataway, NJ, USA: IEEE; 2020. pp. 1-5

[55] Oliveira A, Pedrosa D, Santos T, Dias A, Amaral G, Martins A, et al. Design and development of a multi rotor UAV for oil spill mitigation. In: OCEANS 2019-Marseille. Piscataway, NJ, USA: IEEE; 2019. pp. 1-7

[56] Wu CH, Hsieh JW, Wang CY, Ho CH. Marine pollution detection based on deep learning and optical flow. In: 2020 International Computer Symposium (ICS). Piscataway, NJ, USA: IEEE; 2020. pp. 376-381

[57] De Kerf T, Gladines J, Sels S, Vanlanduit S. Oil spill detection using

machine learning and infrared images. Remote Sensing. 2020;**12**(24):4090

[58] Jiang Z, Zhang J, Ma Y, Mao X. Hyperspectral remote sensing detection of marine oil spills using an adaptive long-term moment estimation optimizer. Remote Sensing. 2021;**14**(1):157

[59] Yin H, Chen S, Huang R, Chang H, Liu J, Qi W, et al. Real-time thickness measurement of marine oil spill by fiber optic surface Plasmon resonance sensors. Frontiers in marine. Riga, LV: Science. 2022;**1937**

[60] Li Y, Yu Q, Xie M, Zhang Z, Ma Z, Cao K. Identifying oil spill types based on remotely sensed reflectance spectra and multiple machine learning algorithms. IEEE Journal of Selected Topics in Applied Earth Observations and Remote Sensing. 2021;**14**:9071-9078

[61] Dala A, Arslan T. In situ microwave sensors and switching circuit for oil slick thickness measurement. IEEE Sensors Journal. 2022;**22**(9):9027-9034

[62] De Carolis G, Adamo M, Pasquariello G. On the estimation of thickness of marine oil slicks from sun-glittered, near-infrared MERIS and MODIS imagery: The Lebanon oil spill case study. IEEE Transactions on Geoscience and Remote Sensing. 2013;**52**(1):559-573

[63] Jorgensen SE, editor. Encyclopedia of Environmental Management, Four Volume Set. Boca Raton, FL, USA: CRC Press; 2012

[64] Yadav M, Sharma D, Sharma O. Propagation of electromagnetic waves in multilayer structure. IJRREST: International Journal of Research Review in Engineering Science and Technology. 2013;**2**:81-82

[65] Hammoud B, Mazeh F, Jomaa K, Ayad H, Ndadijimana F, Faour G, et al. Multi-frequency approach for oil spill remote sensing detection. In: 2017 International Conference on High Performance Computing & Simulation (HPCS). Piscataway, NJ, USA: IEEE; 2017. pp. 295-299

[66] Ulaby FT, Long DG, Blackwell WJ, Elachi C, Fung AK, Ruf C, et al. Microwave Radar and Radiometric Remote Sensing. Ann Arbor, MI, USA: University of Michigan Press; 2014

[67] Hammoud B, Daou G, Wehn N. Multidimensional minimum Euclidean distance approach using radar Reflectivities for oil slick thickness estimation. Sensors. 2022;**22**(4):1431

[68] Muntini MS, Pramono YH, Minarto E, Kalsum U, Rachmanita RE. Modeling and simulation of microwave propagation on crude oil heating. In: 2017 International Seminar on Sensors, Instrumentation, Measurement and Metrology (ISSIMM). Piscataway, NJ, USA: IEEE; 2017. pp. 46-50

[69] Hammoud B, Ndagijimana F, Faour G, Ayad H, Jomaah J. Bayesian statistics of wide-band radar reflections for oil spill detection on rough ocean surface. Journal of Marine Science and Engineering. 2019;**7**(1):12

[70] Hammoud B, Mazeh F, Jomaa K, Ayad H, Ndagijimana F, Faour G, et al. Dual-frequency oil spill detection algorithm. In: 2017 Computing and Electromagnetics International Workshop (CEM). Piscataway, NJ, USA: IEEE; 2017. pp. 27-28

[71] Hammoud B, Faour G, Ayad H, Ndagijimana F, Jomaah J. Performance analysis of detector algorithms using drone-based radar systems for oil spill detection. Multidisciplinary Digital

Publishing Institute Proceedings. 2018;
2(7):370

[72] Hammoud B, Wehn N. A maximum
A-posteriori probabilistic approach using
UAV- nadir-looking wide-band radar for
remote sensing oil-spill detection. In:
2022 International Geoscience and
Remote Sensing Symposium (IGARSS).
Piscataway, NJ, USA: IEEE; 2022.
pp. 7823-7826

[73] Hammoud B, Ayad H, Fadlallah M,
Jomaah J, Ndagijimana F, Faour G. Oil
thickness estimation using single-and
dual-frequency maximum-likelihood
approach. In: 2018 International
Conference on High Performance
Computing & Simulation (HPCS).
Piscataway, NJ, USA: IEEE; 2018.
pp. 65-68

[74] Daou G, Maroun CB, Hammoud B.
Advanced iterative multi-frequency
algorithm used by radar remote-sensing
Systems for oil-Spill Thickness
Estimation. In: 2021 International
Conference on Electrical, Computer and
Energy Technologies (ICECET).
Piscataway, NJ, USA: IEEE; 2021. pp. 1-6

[75] Maroun CB, Daou G, Hammoud B,
Hammoud B. Machine learning using
support vector regression in radar
remote sensing for oil-spill thickness
estimation. In: 2021 18th European Radar
Conference (EuRAD). Piscataway, NJ,
USA: IEEE; 2022. pp. 221-224

[76] Hammoud B, Maroun CB, Ney J,
Wehn N. Artificial neural networks-
based radar remote sensing to estimate
geographical information during oil-
spills. In: 2022 European Signal
Processing Conference (EUSIPCO).
Piscataway, NJ, USA: IEEE; 2022

[77] Hammoud B, Jomaa K,
Ndagijimana F, Faour G, Ayad H,
Jomaah J. Experimental validation of
algorithms used by radar remote-sensing
systems for oil-spill detection and
thickness estimation. In: 2019 16th
European Radar Conference (EuRAD).
Piscataway, NJ, USA: IEEE; 2019.
pp. 205-208

[78] Hammoud B, Ndagijimana F, Faour G,
Ayad H, Fadlallah M, Jomaah J. Reflection-
coefficient experimental extraction from
S21-parameter for radar oil-spill detection
application. Satellite. Oceanography and
Meteorology. 2018;**3**(2):5-6

[79] Hou Y, Li Y, Liu B, Liu Y, Wang T.
Design and implementation of a coastal-
mounted sensor for oil film detection on
seawater. Sensors. 2017;**18**(1):70

[80] Texeira CC, Siqueira CY, Neto FR,
Miranda FP, Cerqueira JR,
Vasconcelos AO, et al. Source
identification of sea surface oil with
geochemical data in Cantarell, Mexico.
Microchemical Journal. 2014;**117**:202-213

[81] Salberg AB, Larsen SØ. Classification
of ocean surface slicks in simulated
hybrid-polarimetric SAR data. IEEE
Transactions on Geoscience and Remote
Sensing. 2018;**56**(12):7062-7073